Cell. Mol. Life Sci. 65 (2008) 312 – 323
1420-682X/08/020312-12
DOI 10.1007/s00018-007-7491-2

Cellular and Molecular Life Sciences

Research Article

A molecular pin to study the dynamics of β-barrel formation in pore-forming toxins on erythrocytes: a sliding model

G. Viero[a,*], A. Gropuzzo[a], O. Joubert[b,+], D. Keller[b], G. Prévost[b] and M. Dalla Serra[a]

[a] FBK-CNR Institute of Biophysics, Unit at Trento, Via alla Cascata 56/C, 38100 Povo (Trento) (Italy), Fax: +39 0461 314875; e-mail: viero@fbk.eu
[b] UPRES EA-3432, Institut de Bactériologie, Faculté de Médecine Université Louis Pasteur – Hôpitaux Universitaires, Strasbourg (France)

Received 22 October 2007; received after revision 15 November 2007; accepted 19 November 2007
Online First 15 December 2007

Abstract. γ-Hemolysins are pore-forming toxins which develop from water-soluble monomers by combining two different 'albeit homologous' proteins. They form oligomeric pores in both cell and model membranes by undergoing a still poorly understood conformational rearrangement in the stem region. The stem is formed by three β-strands, folded onto the core of the soluble protein and completely extended in the pore. We propose a new model to explain such a process. Seven double-cysteine mutants were developed by inserting one cysteine on the stretch that links the β-hairpin to the core of the protein and another on different positions along the β-strands. The membrane bound protein was blocked in a non-lytic state by S–S bond formation. Six mutants were oxidized as inactive intermediates, but became active after adding DTT. These results demonstrate that the stem extension can be temporarily frozen and that the β-barrel formation occurs by β-strand concerted step-by-step sliding.

Keywords. Pore-forming toxin, hemolysin, β-barrel, membrane protein, protein motion.

Introduction

Pore-forming toxins (PFTs) are proteins produced and released by several organisms. They spontaneously combine and insert their stem into the target cell membrane. These proteins share a mechanism of action that could be summed up in four steps: (i) release of soluble monomeric proteins by the bacterium, (ii) binding of the monomers to the target membrane, (iii) oligomerization in a non-lytic prepore, (iv) insertion of the transmembrane β-barrel into the lipid bilayer and opening of the pore [1]. Bi-component γ-hemolysins HlgA-HlgB and α-HL are PFTs secreted by *Staphylococcus aureus* and represent a privileged model to understand and clarify the molecular mechanism of protein-protein and protein-membrane interactions. In fact, structural data are available for the soluble form of HlgB, LukF-PV, LukS-PV [2–4] and for the α-HL transmembrane heptamer [5]. These toxins are closely related both for biological activity and structural rearrangements, despite a quite low sequence identity [6, 7].

Conformational changes accompanying the mode of action of bi-component leucotoxins require self-assembly by non-covalent interaction of six or eight monomers to form an oligomeric alternated pore [8–12]. Three β-strands of each protein constitute the so-called stem domain in solution, which undergoes

+ Present address: CNRS UMR 6548 Université de Nice – Sophia Antipolis Parc Valrose, Nice (France).
* Corresponding author.

major conformational changes during pore formation. The insertion of amphiphilic β-hairpins into the hydrophobic core of the lipid bilayer gives rise to a stable and structured β-barrel. The rearrangements involved in pore formation should permit transition from the starting structures represented by HlgB, LukS-PV or LukF-PV in solution to the final mature pore represented by the α-HL 3D structure. In the soluble form the stem region is completely folded on the β-sandwich, composed of three anti-parallel β-strands (Fig. 1A, B) [2–4], while it evolves into a β-hairpin in the transmembrane form (Fig. 1C). Although much information on the starting and end points in the mechanism of action is available, the time course of the process leading to rearrangement and insertion into the lipid bilayer is still unknown [2, 3]. In fact, collecting data on this time course is difficult since insertion of the transmembrane β-barrel is a fast and cooperative process [13–15]. Furthermore, intermediates occurring during the transition from the soluble to the transmembrane configuration state are not stable [16, 17].

A number of mutants arrested at an intermediate stage, i.e. at the non-lytic prepore state, were already identified and characterized for many PFTs. Moreover, introduction of disulphide bonds (S–S) has been used to clarify the role of the β-barrel of staphylococcal PFTs [18, 19], cytolysin of *Vibrio cholerae* [20], perfringolysin O [13] and of the α-PFT equinatoxin II [21]. Previous results obtained from a disulphide bond-engineered α-HL and a double-cysteine stem mutant of γ-hemolysin demonstrated that conformational stem rearrangements are critical for the β-barrel formation, but not for the binding and the oligomerization [15, 18, 19]. The introduction of a S–S bond constraint between β-strands 7′ and 8 (residues T117 and T136) in the soluble monomer prevents transmembrane β-barrel insertion [19], suggesting that these strands move freely. In both studies the S–S bond was introduced in solution, i.e. at the initial stable stage. A double-cysteine mutant of α-HL, whose mutated residues correspond to those of HlgB, is normally active on red blood cells [18].

An original method proposed here is to arrest intermediates by introducing an S-S bond in double-cysteine mutants of HlgB at different and normally unstable stages during β-hairpin formation. The substituted amino acids were selected in the stem region and far enough in both the soluble and the transmembrane form to avoid S–S bond formation in these stable configurations. Thus, the two cysteines could only react when proximal to each other during the conformational rearrangements leading to β-barrel formation, in this way freezing the process. Furthermore, the two selected cysteines can be used as relative position markers.

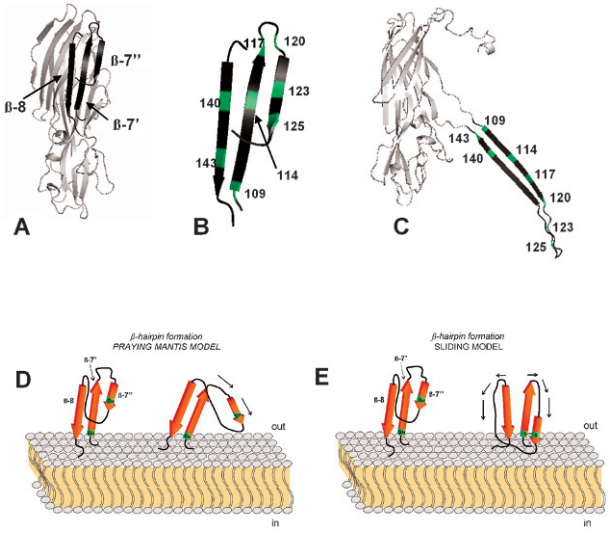

Figure 1. Position of amino acid substitutions. In panel *A* the stem region of HlgB monomer is colored in dark grey (pdb code: 1LKF). In panel *B* mutated positions in the prestem region of HlgB in solution and corresponding residues in the monomer extracted by α-HL transmembrane heptamer (panel *C*, pdb code 7AHL) are colored in green. The following correspondences between γ-hemolysin and α-HL amino acids were considered (Q109 to E111, L114 to L116, T117 to G119, G120 to G122, S123 to T125, S125 to D127, E140 to H144 and N143 to K147). In panel *D* and *E* the cartoons of the stem region explain the two hypotheses used to study the process of stem extension. According to praying mantis hypothesis (*D*) the β-strands extend and penetrate into the lipid bilayer as a desk-lamp-arm turns, following the direction of the black arrows. Since two cysteines (depicted in green in two different positions along the prestem) do not pass one proximal to the other during the conformational changes leading to the β-hairpin formation, S–S bond formation is not allowed. The sliding model (*E*) hypothesizes the opening of the β-strands as a zip (see the direction of the black arrows). In the meantime, they slide downwards in a telescope-like opening. Two cysteines could form a S–S bond when one is in proximity to the other, in this way freezing the extension process. Only in this case does the introduction of a molecular pin enable γ-hemolysin intermediates to be stabilized.

The data presented herein demonstrate (i) stabilization of normally short-lived γ-hemolysin intermediates; ii) the control of β-barrel formation; and (iii) modeling of stem extension during transmembrane β-barrel insertion of γ-hemolysin on the cell membrane. Such a model could be representive of a general mechanism common to other β-barrel PFTs.

Materials and methods

Materials. Egg-PC and cholesterol (chol) from Avanti Polar Lipids (Alabaster, AL, USA) were used for large unilamellar vesicle (LUV) preparation. 1,2-diphytanoyl-sn-glycerophosphocholine (DPhPC) from Avanti Polar Lipids was used for planar lipid

membrane experiments. Triton X-100 was from Merck (Darmstadt, Germany); calcein, EDTA, Sephadex G-50 medium, 1,10-phenanthroline monohydrate and DTT were from Sigma, and $CuSO_4$ was from Carlo Erba (Milan, Italy).

Bacterial strains and vectors. *Escherichia coli* XL1 Blue cells (Stratagene, Amsterdam, Netherlands) were used as recipient cells after site-directed mutagenesis of recombinant plasmids. *E. coli* BL21 was used for overexpression of the pGEX-6P-1-encoded glutathione-S-transferase (GST) leucotoxin fusions as recommended (GE Healthcare, Saclay, France) [22].

Construction and purification of point-mutated X-Cys mutants. The choice of residues for amino acid substitution to cysteine is described in detail in the 'Results' section. Open-reading frames of the secreted HlgA- and HlgB-encoding genes were previously cloned into the expression pGEX-6P1 vector [22, 23]. Recombinant HlgA and HlgB and the 12 HlgB mutants were further obtained by site-directed mutagenesis performed on double-stranded plasmids by using Phusion DNA polymerase (New England Biolabs) and purified as previously described [11]. After removing the GST tag with Prescission Protease (Amersham Pharmacia), HlgA proteins were further purified using cation-exchange FPLC MonoS chromatography (GE Healthcare, Saclay, France) [10]. Homogeneity of proteins dialyzed against 20 mM HEPES, 0.5 M NaCl, 1 mM DTT, pH 7.5 was controlled using SDS-PAGE before they were stored at −80 °C.

Determination of hemolytic activity. Spontaneous HlgB-HlgB dimer formation was checked using SDS-PAGE before determining biological activity (data not shown). Intermolecular oxidation of cysteines was only observed in B109–123. All the mutants were pretreated with DTT 20 mM for 30 min to keep cysteines in a reduced form. Excess reducing agent was removed by gel filtration. RRBCs and HRBCs were used to test mutant activity. RRBCs were purchased from Zootecnica 'Il Gabbiano' (Casole d'Elsa, Siena, Italy), and HRBCs were obtained from fresh blood as described earlier [24]. The time course of hemolysis was determined from the turbidity at 650 nm in a 96-well microplate reader (UVmax, Molecular Devices, Sunnyvale, CA, USA) for 45 min. Toxins were twofold serially diluted in the buffer used for washing (140 mM NaCl, 10 mM Tris-HCl, pH 7.4 for HRBCs and 100 mM NaCl, 30 mM Tris-HCl, 0.1 mM EDTA pH 7.0 for RRBCs). Erythrocytes, at a 0.13 % (v/v) concentration, were added immediately before starting kinetic measurement. The percentage of hemolysis (%HA) was calculated as

$$\%\,HA = 100 \cdot (A_i - A_f)/(A_i - A_w) \quad (1)$$

where A_i and A_f are the absorbances at the beginning and at the end of the reaction, and A_w is the absorption after complete lysis of cells in pure water.

To oxidize the membrane-bound mutants, a suspension of HRBCs or RRBCs at 1.3 % (v/v) was used. Each sample, comprising of 250 µl HRBCs (or RRBCs) and toxins (HlgA WT and HlgB WT or HlgB mutant at equinanomolar concentration), underwent four sequential incubations. Each incubation was followed by centrifugation at 4250 *g* for 1 min to separate cells from the supernatant. The percentage of hemolysis was calculated as the percentage of hemoglobin released in the supernatant following Equation 1. In this case, A_i is the absorbance at 405 nm of the buffer solution (140 mM NaCl, 10 mM Tris-HCl, pH 7.4); A_w is the absorbance after complete lysis of cells in pure water; and A_f is the absorbance at 405 nm of the supernatant obtained after centrifugation at 4250 *g* of 250 µl of a suspension of HRBCs (or RRBCs) and toxins, incubated for 30 min at room temperature.

In order to induce the S–S bond between cysteines, the oxidant Cu^{2+}/phenanthroline was used [21, 25]. The degree of mutant inactivation, induced by oxidant Cu^{2+}/phenanthroline added to the HRBC (or RRBC) suspension in the presence of equimolar concentration of HlgB mutant and HlgA WT, was estimated as

$$\%\ \text{inactivation} = 100 \cdot [1 - \%HA_{ox}/\%HA_{ctr}] \quad (2)$$

where $\%HA_{ox}$ is the summation of the percentages of hemolysis obtained in steps 1, 2 and 3 in the presence of oxidant during step 2, and HA_{ctr} is the sum of the percentages of hemolysis obtained in steps 1, 2 and 3 in the absence of oxidant.

The percentage of recovery describes the ability of the oxidized mutant bound to the erythrocyte plasma membrane to be reduced by DTT. This value was estimated as

$$\%\ \text{recovery} = 100 \cdot (\%HA_{DTT} - \%HA_{ox})/(\%HA_{ctr} - \%HA_{ox}) \quad (3)$$

where $\%HA_{ox}$ is the percentage of hemolysis obtained in steps 1, 2 and 3 in the presence of oxidant during step 2, $\%HA_{DTT}$ is the percentage of hemolysis obtained in steps 1, 2, 3 and 4 in the presence of oxidant during step 2 and 20 mM DTT during step 4, and HA_{ctr} is the sum of the percentages of hemolysis obtained in steps 1, 2 and 3 in the absence of oxidant.

Permeabilization of lipid vesicles. LUVs comprising PC:chol (1:1 molar ratio) were used to check the capability of the mutants to form active pores in model membranes. Liposomes, loaded with 80 mM calcein (a self-quenching condition), were obtained by pneumatic extrusion through two stacked polycarbonate filters with 100 nm pores. LUV diameter was determined by dynamic light scattering using a Malvern ZetaSizer 1000-HS_A (Malvern, UK) as described in [26], and was found to be between 107 and 128 nm. The untrapped dye was removed by gel filtration on a mini-column loaded with Sephadex G-50 gel (Amersham Pharmacia) pre-equilibrated with 10 mM Tris-HCl, 20 mM NaCl, 0.1 mM EDTA pH 7.0. Toxins were serially twofold diluted in the buffer used for gel filtration. Each component had a maximal concentration of protein of 100 nM. Lipid concentration was 5 μM uniformly. Fluorescence intensity at 50 min (F_{fin}) was converted into the percentage of calcein released by comparing it to the maximum signal (F_M), obtained after addition of 1 mM Triton X-100 according to

$$\%R = 100 \cdot (F_{fin} - F_{in}) / (F_M - F_{in}) \quad (4)$$

where F_{in} is the initial fluorescence before addition of toxins.

Planar lipid bilayer experiments. Solvent-free planar lipid membrane (PLM) was made of DPhPC as reported [27]. The protein was only added on one side (*cis*) to stable preformed bilayers. All experiments were conducted in symmetrical starting conditions, i.e. with the same buffer in both chambers (10 mM Hepes, 100 mM KCl, 0.1 mM EDTA pH 7). The *trans* side was at ground.

Macroscopic currents were recorded by a patch clamp amplifier (Axopatch 200, Axon Instruments). A PC equipped with a DigiData 1200 A/D converter [Axon Instruments, now Molecular Devices (Toronto, Canada)] was used for data acquisition. Current traces were filtered at 100 Hz and acquired by computer using Axoscope 8 software (Axon Instruments). Measurements were performed at room temperature.

Kinetic. The time course of hemolysis induced by reactivation of oxidized mutants was followed by measuring turbidity at 650 nm. A suspension of HRBCs with non-lytic oxidized mutants, bound to the membrane and obtained as described in Figure 4, was diluted to a final O.D. of 0.1. Absorbance was measured every 9 s for 45 min after adding 20 mM DTT to each well. The percentage of hemolysis was calculated using (Eq. 1). The maximal rate of hemolysis, V_{max} (mOD/s), was the maximal slope of the O.D. time curve.

Results

Design of double-cysteine mutants. A comparison between the structures of a protomer extracted from the heptameric transmembrane pore of α-HL [5] and the monomer of the soluble leucotoxins (Fig. 1C, A, respectively) [2–4] reveals a common structural organization [7]. The main difference is the location of the β-hairpin, which forms the walls of the β-barrel (Fig. 1A, C, dark grey region). The conformational and spatial modifications occurring during β-barrel formation have still not been described in any PFT model to date [28, 29]. Here we explore two possibilities to explain the stem extension process: (i) β-strands extend and penetrate the lipid bilayer with a reading lamp-arm like movement (praying mantis model, Fig. 1D); (ii) β-strands open as a zip and, at the same time, slide downwards in a telescope-like opening (sliding model, Fig. 1E). These hypotheses can be tested by introducing structural constraints between the triangle region and different positions along β-strands.

Six double-cysteine mutants of HlgB were produced introducing 2 amino acid substitutions, one into the region connecting the β-hairpin to the core of the HlgB protein (Q109C) and the other (Fig. 1A, B) at different positions along β-strand 7′ (L114C and T117C), β-strand 7″ (G120C, S123C and S125C) or β-strand 8 (E140C) [2]. Furthermore, another mutant (BT117C-N143C) was used to demonstrate the relative movement of the β-strands 7′ and 8. In this mutant the fixed amino acid was N143 (Fig. 1B), which is the counterpart of Q109 on the opposite triangle stretch. The following seven double cysteine mutants were therefore obtained: B109–114, B109–117, B109–120, B109–123, B109–125, B109–140 and B117–143. Five HlgB single-cysteine mutants (i.e. at positions 109, 114, 117, 120 and 123) were produced as further controls in addition to native HlgB.

Cysteines in each double mutant were chosen for being 3–10 times farther than the maximum distance allowed for spontaneous S–S bond formation (which is 4–5 Å [30]), both in the soluble and in transmembrane state (Fig. 1A, C).

Activity of double mutants on biological and model membranes. Double-cysteine mutants were tested for their hemolytic and pore-forming activity on model membranes in order to ascertain that amino acid substitutions do not cause loss of lytic ability. Hemolytic activity on human red blood cells was checked in the presence of an equimolar concentration of HlgA WT (with or without DTT), thus preventing dimer or multimer formation by inter-molecular S–S bonding in solution (Table 1). All the mutants retain hemolytic

Table 1. Activity on biological and model membranes of the WT and of double-cysteine mutants.

	Biological membranes		Model membranes	
	HRBCs		LUVs	
	−DTT (C_{50}/nM)[1]	+DTT (C_{50}/nM)	−DTT (C_{50}/nM)[2]	+DTT (C_{50}/nM)
B	10.2 ± 4.1	9.6 ± 1.2	7.7 ± 2.2	7.7 ± 1.2
B109–114	16.4 ± 2.4	13.4 ± 0.6	14.1 ± 0.9	11.5 ± 0.6
B109–117	14.8 ± 7.6	19.5 ± 1.7	12.8 ± 1.5	8.1 ± 1.1
B109–120	5.3 ± 1.0	5.7 ± 0.4	9.5 ± 0.5	7.1 ± 0.9
B109–123	6.5 ± 1.3	8.4 ± 0.2	9.9 ± 1.9	7.3 ± 2.4
B109–125	9.5 ± 0.9	8.4 ± 0.9	7.3 ± 1.4	6.7 ± 0.7
B109–140	9.0 ± 2.0	8.0 ± 0.1	10.5 ± 1.4	9.8 ± 2.3
B117–143	9.5 ± 1.5	7.0 ± 0.2	10.1 ± 1.4	10.1 ± 0.8

[1] C_{50} are the mean ± sd of 3–7 independent experiments
[2] C_{50} are the mean ± sd of 3–5 independent experiments

activity. Nevertheless, B109–120 and B109–123 display a slightly lower C_{50} value, while B109–114 and B109–117 show decreases in activity that are not statistically significant and were therefore not further investigated. Statistical analysis was carried out using the unpaired Student's *t* test, $p < 0.05$ was considered significant. Double mutants B109–140, B117–143 and B109–125 are as active as the native protein. The presence of a reducing agent (data not shown) as the preincubation with DTT 20 mM for 30 min does not lead to an increase in hemolysis, suggesting the absence of spontaneous S–S bond formation at 25 °C before or during β-barrel insertion (Table 1). The same experiments were performed on RRBCs with the same results, and for this reason they are not shown.

Permeabilizing activity of double mutants was determined on liposomes composed of PC:chol (1:1 molar ratio) (Table 1), which has been shown to be the most sensitive lipid composition for this toxin [24]. In the presence of equimolar concentration of HlgA WT, B109–120, B109–123 and B109–125 are able to permeabilize liposomes just as WT does. On the contrary, B109–114, B109–117, B109–140 and B117–143 are slightly less active. Except for WT and B117–143, a slight increase in activity is observed in the presence of DTT. Nevertheless, such an enhancement of pore activity could be due to a slightly inter- or intrachain spontaneous S–S bond formation.

In order to ascertain whether the mutant pore resembles the WT architecture, electrophysiological properties on PLMs were evaluated. In the presence of HlgA WT all the mutants are able to open pores in planar membranes composed of DPhPC (Fig. 2 and Table 2). In 100 mM KCl mutant pores normally stay open most of the time as the native couple [8, 31] and α-HL is not exception [32]. Some partial closures or opening events are observed at +40 mV for mutants B109–114, B109–117, B109–120, B109–123 and B117–143, suggesting that these pores could be less stable than the WT on planar membranes (Fig. 2). Since the pores formed by single mutant B109 stay open most of the time [unpublished results], residue Q109 alone is not involved in this instability. A direct interaction of residue T117 of α-HL with lipids was demonstrated [33], suggesting that residues along the β-hairpin could play a role in β-barrel stabilization. Mean conductance values of the mutants (Table 2) show a certain variability. The lowest conductance is 102 pS (B109–117) and the highest is 161 and 160 pS (B109–140 and B117–143, respectively). As already demonstrated [31], substitutions of amino acids facing the lumen of the pore could affect electrophysiological properties of the channel rather than the pore structure. In the hypothesis of a cylindrical pore filled with water molecules, different conductances rely on small variations in the pore diameter (10 % of wild-type pores, as reported in Table 2 legend).

In conclusion, biological activity in mutants and in the WT is very similar, and the introduction of two cysteines does not extensively affect the overall structure of the pore. Moreover, the S–S bond does not form spontaneously, as shown by hemolytic and permeabilizing activities, which are very similar whether the reducing agent is present or not. Therefore, we propose two alternative explanations: (i) intramolecular cysteines do not pass close enough to each other to allow S–S bond formation at all or (ii) cysteines do pass close to each other during β-barrel insertion, but too rapidly, therefore not allowing formation of an S–S bond.

Reversible and temperature-dependent arrest of pore formation. Once the monomer has bound to the target

Table 2. Electrophysiological parameters of the WT and of double cysteine mutants.

	G[1] (pS)	I^+/I^-[2]	% Δd[3]
B	128 ± 13 *(608)*	0.41 ±0.05 (8)	–
B109–114	114 ± 11 *(72)*	0.38 ± 0.04 (6)	6
B109–117	102 ± 37 *(133)*	0.40 ± 0.07 (3)	11
B109–120	132 ± 15 *(72)*	0.40 ± 0.01 (2)	2
B109–123	116 ± 18 *(618)*	0.37 (1)	2
B109–125	128 ± 46 *(163)*	0.49 (1)	5
B109–140	161 ± 15 *(94)*	0.51 ± 0.04 (2)	12
B117–143	160 ± 46 *(93)*	0.50 ± 0.04 (2)	12

[1] Single-channel conductance at + 40 mV. Values are the mean ± sd. The number of events is shown in brackets.
[2] Mean values of the ratio between ion current flowing through a single channel at positive and negative voltages (± 120 mV). The number of independent experiments is shown in brackets.
[3] Variation in diameter (Δd) of the pores formed by mutants with respect to that of the WT. Δd was estimated as follows:
$\% \Delta d = |d_{mut} - d_{WT}| / d_{WT} \cdot 100$ [A]
where d_{mut} is the diameter of the pore formed by the WT couple and d_{WT} is the diameter of the pore formed by the mutant. The diameter of the pore d is correlated to conductance by
$d = (2 G l \pi^{-1} \sigma^{-1})^{1/2}$ [B]
where G is the mean conductance of pores as described in Table 2, σ is the conductivity of the buffer solution during the experiment and l is the length of the pore. Substituting Equation B in Equation A we obtain
$\% \Delta d = |1 - (G_{mut}/G_{WT})^{1/2}| \cdot 100$.

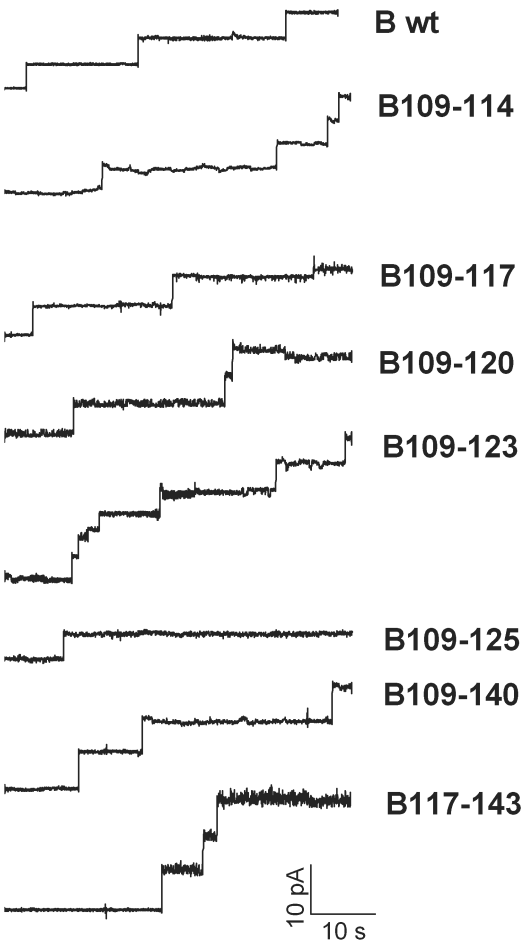

Figure 2. Pore formation on planar lipid membranes by double-cysteine mutants. Representative stepwise current increases corresponding to the opening of single-ion channels of HlgB double-cysteine mutants and WT as indicated on the right of each trace. Each protein was added to the *cis* side at concentrations between 1 and 20 nM in the presence of equimolar HlgA WT. The applied voltage was +40 mV in all cases. The height of each step was used to calculate the conductance of that pore as reported in Table 2.

membrane, the stem region is still exposed to the hydrophilic environment and therefore accessible to proteinase and to attack of sulphydryl reagents [16]. Hence, we propose a novel method of oxidizing cysteines in the membrane-bound protein, which becomes non-lytic. The process of membrane binding could be dissociated from pore formation by lowering the temperature to 4 °C [19, 24]. At this temperature, monomers are able to bind normally to the plasma membrane, while the transmembrane insertion of the β-barrel is prevented. Pore formation should occur only after raising the temperature to 25 °C [19, 24]. Therefore, the ability of double mutants to become temporarily non-lytic at 4 °C (in the presence of HlgA WT and HRBCs) was verified. The incubation time of the toxin and erythrocytes at 4 °C was 30 min. All the mutants show temperature-dependent inhibition of pore formation (Fig. 3A, dashed bar), with a percentage of hemolysis lower than 13 %. The unbound protein was removed by centrifugation at 4 °C, and pore formation ability was re-established by resuspending the pellet in a toxin-free buffer at 25 °C for 30 min, which is enough for pore formation. After raising the temperature to 25 °C (Fig. 3A, grey bar), hemolysis is observed for all the mutants. B109–125 and B117–143 reach only 40 and 45 % of hemolysis in 30 min. The difference in hemolytic activity between these mutants and the WT is statistically significant (B109–125 $p = 0.0002$ and B117–143 $p = 0.02$) and is due to their lower binding ability to erythrocytes [A. Gropuzzo personal communication]. Indeed, the observed hemolysis is suggestive of absence of spontaneous S–S bond formation, both in solution and during stem rearrangements. Therefore, S–S bond formation is favored by oxidant addition.

Arrest of stem extension by S–S bond formation in membrane-bound mutants. Using inhibition of pore formation by low temperature, HlgB mutants were oxidized when bound to the plasma membrane. The same sample of HRBCs and toxin was treated as follows: (1) monomer binding to erythrocytes at 4 °C (step 1, Fig. 3B); (2) cysteine oxidation (using Cu^{2+}/phenantholine, thereafter removed by centrifugation) at 4 °C, before pore formation (step 2, Fig. 3B); (3)

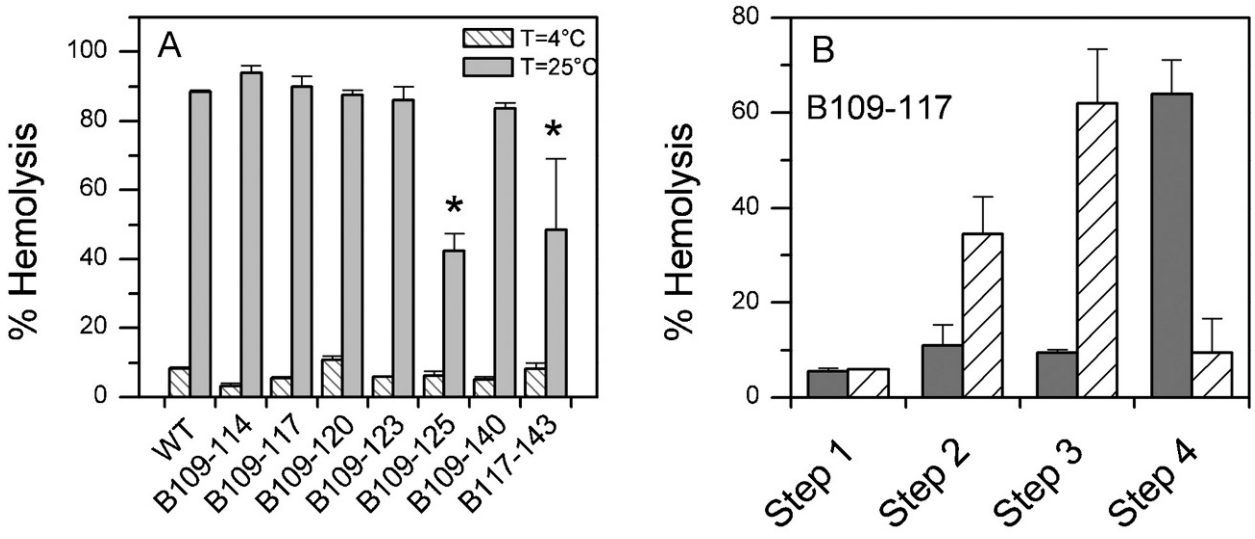

Figure 3. Temperature-dependent hemolytic activity of mutants and of the WT and arrest of pore formation by oxidation. In (*A*) all the mutants and WT (10 nM), incubated with an HRBC suspension (O.D. = 1), are not hemolytic at 4 °C (dashed bars). After removing the unbound protein by centrifugation and raising the temperature to 25 °C, they become hemolytic (grey bars). The percentage of hemolysis was calculated from the amount of hemoglobin released after raising the temperature and spinning down the RBC suspension. Statistical analysis was carried out by using the unpaired Student's *t* test. $p < 0.05$ was considered significant. Each bar represents the mean ± sd of 3–4 independent experiments, * $p < 0.05$. In (*B*) oxidation of mutant B109–117 after binding to HRBC plasma membrane (grey bars) and control in the absence of oxidant (dashed bars). *Step 1:* binding of the toxin to the membrane. HlgA WT (10 nM) and B109–117 (10 nM) were added to an HRBCs suspension (O.D. = 1) and incubated for 30 min on ice. Intact erythrocytes formed a pellet after centrifugation, and the released hemoglobin was measured. At 4 °C, the hemolysis is less than 6 %. *Step 2:* Cysteine oxidation. The pellet from step 1, which was always maintained at 4 °C, was incubated for 30 min with (grey bar) or without (dashed bar) Cu^{2+}/phenanthroline (6 mM). This is a well-known oxidizing agent used for improving the yield of S–S bond formation [21, 45, 46]. The sample was centrifuged and the absorbance of hemoglobin released in the supernatant is measured at 405 nm. *Step 3:* Pore formation and/or blockage observation. Buffer at room temperature was added to the pellet from step 2: the raising of the temperature triggers oligomerization and eventually pore formation. After 30 min the suspension was centrifuged and the absorbance of hemoglobin present in the supernatant was measured. The absence of hemolysis suggests that pore formation does not occur when the mutant is treated with the oxidant (grey bar), while in the control without Cu^{2+}/phenanthroline (dashed bar) the mutant is able to induce hemolysis. *Step 4:* Blockage removal with DTT at room temperature. The pellet from step 3 was subjected to DTT (20 mM final), and the released hemoglobin was measured from the supernatant as in the previous steps. Mean ± sd of 4 experiments is reported.

pore formation and/or inhibition of hemolysis at 25 °C (step 3, Fig. 3B); (4) constraints removal by S–S bond reduction at 25 °C (step 4, Fig. 3B) (for experimental details, see the legend in Fig. 3B). After each step, the sample was centrifuged to measure hemoglobin released into the supernatant and to collect the intact erythrocytes.

As an example, the data collected at each step with B109–117 in oxidizing condition are shown in Figure 3B (grey bars). In the control experiment (in the absence of oxidant, dashed bars), the increase in temperature triggers pore formation, which causes 60 % of hemolysis, as reported in Figure 3B. In contrast oxidant addition at 6 mM caused clear inactivation that could be already be observed at step 2 and at room temperature (Fig. 3B, grey bar, steps 2 and 3). Addition of DTT (step 4) activated the process which leads to hemolysis, suggesting that pore formation, i.e. assembly and formation of a transmembrane β-barrel, is arrested until reduction of the S–S bond.

The oxidizing method has been applied to double mutants as well as to the WT couple and to single mutants (B109, B114, B117, B120 and B123) as controls. Starting from the percentages of hemolysis caused at each step (Fig. 3B), an estimate of the inactivation degree induced by S–S bond formation was calculated (see 'Materials and methods'). The behavior of B109–140, B109–125 and B117–143 was compared to that of WT and single mutant controls (Fig. 4A) at different toxin/oxidant ratio. B109–140 shows the highest inactivation (80 %) with 10 nM and 6 mM of toxin and oxidant, respectively. The other proteins behave similarly to B109–125, while B117–143 is the least inactivated at all toxin/oxidant ratios tested. The pore-forming ability of the WT couple and single-cysteine mutants is not affected by oxidizing conditions at any toxin/oxidant ratio tested (Fig. 4A). The inactivation value of pore formation for all double mutants is reported in Figure 4B. Six mutants show inactivation ranging from 62 to 82 %. In contrast, the inactivation induced in B117–143 is very low (22 %).

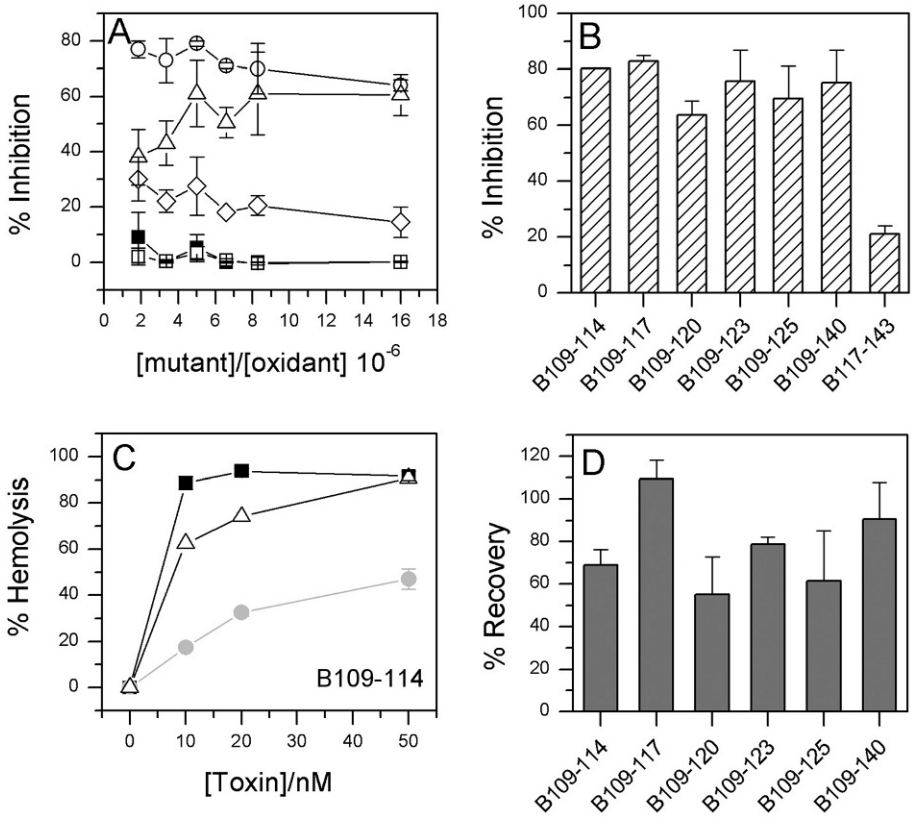

Figure 4. Reversible inactivation of pore-forming activity on HRBCs by S–S bond formation. (*A*) Inhibition of hemolytic activity for some double-cysteine mutants (circles correspond to B109–140, triangles to B109–125, diamonds to B117–143), for the single-cysteine mutants (open squares) and the WT (filled squares), used as controls, at different mutant-to-oxidant ratios. (*B*) Inhibition of all the double cysteine mutants at 3.3 10^{-6}mutant-to-oxidant ratio, calculated following Equation 2 in the 'Materials and methods' section. The mean ± sd of 3–4 experiments is reported. (*C*) Percentage of hemolysis of B109–114 without oxidation of cysteines (open squares), after step 3 (see Fig. 3 legend) of the oxidation protocol (gray circles) and, finally, after DTT addition (filled squares). The Cu^{2+}/phenanthroline concentration during step 2 was 6 mM. The mean of 4 experiments is reported; sd does not exceed 15%. (*D*) Residual hemolysis after 20 mM DTT addition to the mutants bound to the erythrocyte membranes and oxidized as described in the legend to Figure 3. The percentage of recovery was calculated by Equation (3) in the 'Materials and methods' section. The mutant-to-oxidant molar ratio is 3.3 10^{-6}. Mean ± sem of 3–5 experiments is reported.

After addition of DTT, mutants recover their hemolytic activity, as shown in Figure 4C and D, confirming the presence of a reducible bond. Similar behavior was also observed by [19, 34], supporting S–S bond-dependent inactivation. The percentage of recovery for B117–143 is very low because this mutant is slightly oxidized. Therefore, this mutant induces complete hemolysis before addition of the reducing agent.

Depending on the relative position of the two cysteines, the capability of double-cysteine mutants to form intramolecular S–S bonds is demonstrated. These results prove that the introduction of a constraint at the stem level impairs the complete transmembrane insertion of the β-barrel till addition of a reducing agent. These experiments display the same behavior on RRBCs (not shown).

Switching on stem insertion under reducing conditions. Stabilization of subsequent intermediates during β-barrel extension and isolation of activable pores by chemical control open the possibility of studing the kinetic of β-hairpin insertion into the membrane. Here, the rate of hemolysis after DTT addition to four oxidized mutants (B109–114, B109–117, B109–120 and B109–123) has been studied. According to the sliding model hypothesis and depending on amino acid substitutions (as depicted in Fig. 1A–C), S–S bond position should be different for each mutant. Therefore, each β-hairpin is arrested at a different step of the extension process by the formation of a loop at the stem level. The length of the loop is dependent on the relative position of cysteines (4, 7, 10 and 13 residues for B109–114, B109–117, B109–120 and B109–123, respectively). The S-S bond may act as a pin at different degrees of the stem reorganization, before β-hairpin extension is completed. Consequent-

ly, the greater the loop is, the slower reorganization and S–S bond accessibility will be and, therefore, the longer the time for reactivation.

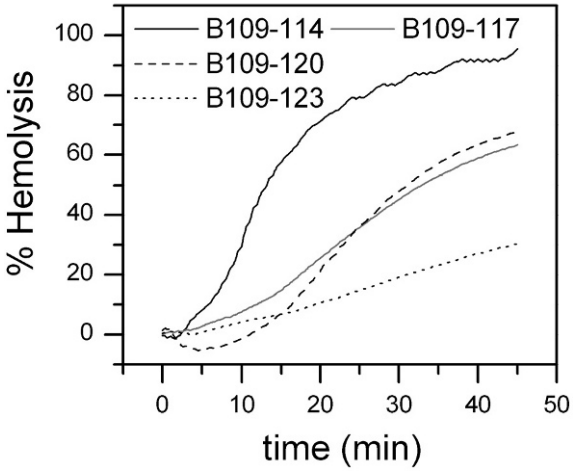

Figure 5. Time course of the recovery of hemolytic activity. The pellet from Figure 2, step 3, was dispensed in a microplate, and hemolysis was measured immediately after addition of 20 mM DTT. The reported kinetics represent a typical experiment. These time courses have been repeated 2–4 times, giving similar results.

All the traces reported in Figure 5 show a delay in hemolysis, which is similar to what has already been described by [19] for a stem-stem mutant after β-mercaptoethanol addition. Hemolysis, in its early stages, is a pore-forming-dependent process and is related to S–S bond accessibility and reduction. In fact, diffusion of DTT in solution is equal for the four double mutants, allowing comparison of the kinetic parameters (Table 3). The time necessary to reach 50 % (t_{50}) of hemolysis after DTT addition is 20–50 min and is dependent on the position of the second cysteine (residue 109 being fixed for the mutants tested) along the β-strand, giving the time scale order L114C < T117C < G120C < S123C. B109–114 shows the lowest value, while B109–123 shows the highest. Immediately after DTT addition, B109–120 displays an apparent decrease in hemolytic activity which can probably be ascribed to a slight swelling of cells. Nevertheless, once hemolysis has begun, this mutant reaches 50 % of hemolysis faster than B109–123 (Fig. 5 and Table 3). The maximal rate of hemolysis of the reduced mutants compared to that of the control shows the same time-scale order: B109–114 being the fastest ($V1_{max} = 0.061$ mOD s^{-1}) and B109–123 the slowest ($V1_{max} = 0.010$ mOD s^{-1}).

Finally, these results support sliding of the β-strands as a step-by-step process and represent one of the first descriptions of the time course of the staphylococcal β-barrel extension into the membrane.

Table 3. Kinetic parameters of four oxidized double mutants after reduction of the S–S bond.

Mutant	t_{50} (min)	$V1_{max}$ [1] (mOD/s)	$V2_{max}$ [2] (mOD/s)	$V1_{max}/V2_{max}$
B109–114	22.8	0.061	0.056	1.1
B109–117	38.7	0.027	0.050	0.5
B109–120	44.5	0.029	0.095	0.3
B109–123	> 50.0	0.010	0.065	0.1

[1] $V1_{max}$ is the maximal rate of oxidized mutant after DTT addition.
[2] $V2_{max}$ is the maximal rate for non-oxidized mutants.
All the parameters are the mean of 2–4 independent experiments.

Discussion

β-Barrel PFTs can spontaneously form oligomeric transmembrane pores by a concerted process that does not require any metabolic energy. Each step in the mechanism of action requires conformational changes which occur in the quaternary (oligomerization), tertiary and secondary structure (β-barrel formation). Up to eight β-hairpins need to move and tilt by about 180° with respect to the main protein axes to penetrate the membrane with a very fast movement, causing hemolysis in few seconds [13]. The dynamics and protein motions proposed for membrane proteins such as aspartate receptor and acetylcholine nicotinic receptor [29] could not explain the stem extension of β-PFTs. Moreover, these protein motions are small and concern already inserted α-helices. Studies on β-sheet formation in model membranes were proposed using small peptides which do not form pores and represent a very simplified protein model [35–37]. The β-barrel refolding of bacterial outer membrane proteins (Omps) is the most investigated [37] and indicates that β-barrel proteins fold in distinct steps with several intermediates. In this case, β-barrel formation involves the whole protein. On the other hand, only the stem, a small portion of PFTs which accounts for ~10 % of the whole protein, inserts into the lipid bilayer. Neither the movement nor the conformational changes of the stem to form the β-barrel of PFTs in the cell membrane have been studied until now.

Isolation of intermediates in this process was tried out for several β-PFTs [18, 19, 38] by introducing S–S bonds in double-cysteine mutants at the soluble and stable stage. Here, in order to investigate the dynamics of β-barrel formation, unstable intermediates of HlgB were stabilized by introducing an S–S bond during the extension process of the β-hairpin in the lipid bilayer. The introduced constraint acts as a molecular pin which impedes pore formation. Seven double-cysteine mutants of HlgB were produced, by placing the mutated residues in the stem region, which undergoes

conformational rearrangements to form a β-barrel. The mutated amino acids are distant from each other in both the soluble and the transmembrane stage.

The activities on biological and model membranes are very similar to that of the WT (Tables 1 and 2), confirming that the amino acid substitutions do not affect pore-forming ability. Thus, we may assume that the pore architecture of the mutated proteins resembles that of the native pore.

By oxidation, the conformational rearrangements of the stem are impeded in six of the seven double-cysteine mutants (Figs. 3B, 4B). According to the sliding model and not to the praying mantis one, this result suggests that cysteines become able to interact only after binding of the protein to the membrane. In principle, different Hlg stem regions could interact together, allowing formation of intermolecular S–S bonds between two HlgB mutants. In fact, the secondary structure adopted by stems after the binding of each monomer to the membrane and at the prepore stage remains unknown. The prestem can be still connected to the core of the protein or partially unfolded, lying on the membrane surface as in the model proposed for Omps and α-toxin [37, 39]. Any intermolecular S–S bond formation can be excluded because of (i) the absence of inactivation for the WT and for single-cysteine mutants under oxidizing conditions; (e.g. at the unstable intermediate HlgB-HlgB stage [10]); (ii) the alternate position of HlgA and HlgB in the pore where each HlgB mutant is flanked by two cysteine-less HlgA monomers [9–11].

The sliding model, as depicted in Figure 6, is indeed compatible with most of the mutants. Nevertheless, it does not fully explain the low and high oxidation of B117–143 and B109–140, respectively. In fact, comparing the inactivation degree of B117–143 and B109–117, it appears that B117–143 is unaffected by Cu^{2+}/phenanthroline (Fig. 4B). Residue N143, located on β-strand 8 flanking β-strand 7′, faces residue Q109. Thus, mutant B117–143 describes the movement of T117 close to β-strand 8. The low inactivation ability of B117–143 suggests that, during β-barrel insertion, T117 neighbors Q109 rather than N143. During sliding of the β-hairpin, a portion of β-strand 7′ could interpose between N143 and T117, reducing the possibility of S–S bond formation. In contrast, Q109 and T117 are close to each other on the same β-strand 7′, which collapses downwards (Fig. 6), allowing oxidation of the cysteines.

The inactivation ability of B109–140 allows further interesting considerations on the conformational changes of the stem. In the hypothesis of a simple vertical sliding of the strands, E140 should not get close to Q109 (Fig. 6). Nevertheless, contact is possible in the case of a transient overlapping of β-strand 7′ and β-strand 8, which may tilt the stem region during β-barrel insertion. Accordingly, β-strands are inclined at about 40° from the membrane normal [37], and such an inclination of the β-hairpins in the αHL structure was already reported [5], explaining the high degree of S–S bond formation for B109–140.

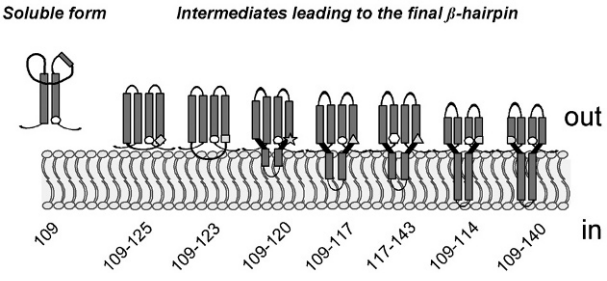

Figure 6. Cartoon of sliding model intermediates. A complete scheme of the stabilized intermediates is depicted based on the sliding model. The time course of stem sliding should evolve from the soluble (on the left) to the transmembrane form (on the right) through 7 intermediates, corresponding to the 7 double mutants. Each intermediate describes the relative positions of cysteines in the stem region and the putative stem extension degree reached before blockage becomes effective. Relative positions of the mutated residues are represented by symbols: circle (Q109C); diamond (S125C); square (S123C); star (G120C); triangle (T117C); hexagon (N143C); left moon (L114); right moon (E140C).

These results suggest that (i) strand 8 is probably far from strand 7′ and could partially lie on the surface of the membrane, buried in the lumen of the prepore; (ii) strands 7′ and 8 display a slightly different pattern of unfolding, consistent with the different behavior of the two β strands in the α-HL oligomer [40]; (iii) before β-barrel formation, strand 8 may collapse and lie on the membrane surface while strand 7′ slides and inserts downwards into the membrane. In such a way the position in the α-HL prepores of residue 130, which does not interact with lipids before β-barrel formation [16], could be explained.

After pin removal by DTT addition, kinetic parameters (Table 3), show a time delay by comparison with controls (i.e. not oxidized mutants). Thus, before β-barrel insertion the strands need more time to correctly reorganize. The same time delay was observed only for β-PFTs with pore entrance size similar to those of staphylococcal PFTs, supporting the idea that a common mechanism may exist and one structure-function relationship could fit different β-PFTs [19, 34, 41].

Our results do not require a complete unfolding and lying of the strands on the membrane surface before β-barrel formation, as hypothesized for OmpA [37] and the α-HL [39] 'molten disk' intermediate. The proposed sliding model depicted in Figure 6 as a simplified cartoon (the organization of the secondary structure in these regions has not yet been deter-

mined) well explains our findings. These are further supported by Nguyen et al. [19], who demonstrated that the two β-strands must move freely to form the transmembrane pore. As a consequence the opening of the strands and the change in the relative positions of the two residues is necessary, and the alternative praying mantis model is no longer tenable. Moreover, the sliding model would be favored in terms of thermodynamics. In fact, interstrand hydrogen bonds in a β-barrel are the predominant stabilizing interactions [37]. Moreover, inter- and intrastrand hydrogen bonds could reorganize in a step-by-step mode while a protein region translocate across the membrane.

In conclusion, a method was developed specifically to block and control γ-hemolysin pore formation into the plasma membrane of erythrocytes, stabilizing six intermediates during β-barrel formation. The results of this study are well explained by a sliding model (at least for β-strand 7′) that describes movement leading to β-barrel assembly that favors a step-by-step downwards sliding and tilt of the stem. Finally, these results highlight a still unknown process for many β-PFTs which share β-barrel structures and a similar pre-stem folding [42]. This model might be proposed as a common mechanism for other β-barrel PFTs, such as anthrax protective antigen [43], *Vibrio cholerae* cytolysin [44] and other membrane proteins.

Acknowledgement. This paper is dedicated to the memory of Gianfranco Menestrina. We thank Maria Luisa Libardi and Andrea Cuppoletti for English proof reading of the manuscript. We thank Gregor Anderluh for his critical reading. This work was granted by a research convention (StaWars project) between Provincia Autonoma di Trento (Italy) and the 'Direction de la Recherche et des Etudes Doctorales' (UPRES EA-3432). O.J. is supported by a grant from a research convention (StaWars project) between Provincia Autonoma di Trento (Italy), and the 'Conseil Régional d'Alsace'. G.V. was supported by a PhD grant from the University of Verona.

1 Parker, M. W. and Feil, S. C. (2005) Pore-forming protein toxins: from structure to function. Prog. Biophys. Mol. Biol. 88, 91–142.
2 Olson, R., Nariya, H., Yokota, K., Kamio, Y. and Gouaux, J. E. (1999) Crystal structure of staphylococcal LukF delineates conformational changes accompanying formation of transmembrane channel. Nat. Struct. Biol. 6, 134–140.
3 Pédelacq, J. D., Maveyraud, L., Prévost, G., Baba-Moussa, L., Gonzalez, A., Courcelle, E., Shepard, W., Monteil, H., Samama, J. P. and Mourey, L. (1999) The structure of a *Staphylococcus aureus* leucocidin component (LukF-PV) reveals the fold of the water-soluble species of a family of transmembrane pore-forming toxins. Structure 7, 277–287.
4 Guillet, V., Roblin, P., Werner, S., Coraiola, M., Menestrina, G., Monteil, H., Prévost, G. and Mourey, L. (2004) Crystal structure of leucotoxin S component: new insight into the staphylococcal beta-barrel pore-forming toxins. J. Biol. Chem. 279, 41028–41037.
5 Song, L., Hobaugh, M. R., Shustak, C., Cheley, S., Bayley, H. and Gouaux, J. E. (1996) Structure of staphylococcal alpha-hemolysin, a heptameric transmembrane pore. Science 274, 1859–1866.
6 Menestrina, G., Dalla Serra, M., Comai, M., Coraiola, M., Viero, G., Werner, S., Colin, D. A., Monteil, H. and Prévost, G. (2003) Ion channels and bacterial infection: the case of beta-barrel pore-forming protein toxins of *Staphylococcus aureus.* FEBS Lett. 552, 54–60.
7 Gouaux, J. E., Hobaugh, M. and Song, L. Z. (1997) Alpha-hemolysin, gamma-hemolysin, and leukocidin from *Staphylococcus aureus:* distant in sequence but similar in structure. Protein Sci. 6, 2631–2635.
8 Miles, G., Movileanu, L. and Bayley, H. (2002) Subunit composition of a bicomponent toxin: staphylococcal leukocidin forms an octameric transmembrane pore. Protein Sci. 11, 894–902.
9 Jayasinghe, L. and Bayley, H. (2005) The leukocidin pore: evidence for an octamer with four LukF subunits and four LukS subunits alternating around a central axis. Protein Sci. 14, 2550–2561.
10 Viero, G., Cunaccia, R., Keller, D., Werner, S., Monteil, H., Prévost, G., Menestrina, G. and Dalla Serra, M. (2006) Homologous versus heterologous interactions in the pore of bicomponent staphylococcal γ-hemolysins. Biochem. J. 394, 217–225.
11 Joubert, O., Viero, G., Keller, D., Martinez, E., Colin, D. A., Monteil, H., Mourey, L., Dalla Serra, M. and Prévost, G. (2006) Engineered covalent leucotoxin heterodimers form functional pores: insights into S-F interactions Biochem. J. 396, 381–389.
12 Joubert, O., Voegelin, J., Guillet, V., Tranier, S., Werner, S., Colin, D. A., Dalla Serra, M., Keller, D., Monteil, H., Mourey, L. and Prévost, G. (2007) Distinction between pore assembly by staphylococcal α-toxin versus leucotoxins. J. Biomed. Biotechnol. ID 25935 1–13.
13 Hotze, E. M., Wilson-Kubalek, E. M., Rossjohn, J., Parker, M. W., Johnson, A. E. and Tweten, R. K. (2001) Arresting pore formation of a cholesterol-dependent cytolysin by disulfide trapping synchronizes the insertion of the transmembrane beta-sheet from a prepore intermediate. J. Biol. Chem. 276, 8261–8268.
14 Valeva, A., Palmer, M., and Bhakdi, S. (1997) Staphylococcal alpha-toxin: formation of the heptameric pore is partially cooperative and proceeds through multiple intermediate stages. Biochemistry 36, 13298–13304.
15 Nguyen, A. H., Nguyen, V. T., Kamio, Y. and Higuchi, H. (2006) Single-molecule visualization of environment-sensitive fluorophores inserted into cell membranes by staphylococcal gamma-hemolysin. Biochemistry 45, 2570–2576.
16 Valeva, A., Palmer, M., Hilgert, K., Kehoe, M. and Bhakdi, S. (1995) Correct oligomerization is a prerequisite for insertion of the central molecular domain of staphylococcal alpha-toxin into the lipid-bilayer. Biochim. Biophys. Acta 1236, 213–218.
17 Vecsey-Semjen, B., Knapp, S., Mollby, R. and van der Goot, F. G. (1999) The staphylococcal alpha-toxin pore has a flexible conformation. Biochemistry 38, 4296–4302.
18 Kawate, T. and Gouaux, E. (2003) Arresting and releasing Staphylococcal alpha-hemolysin at intermediate stages of pore formation by engineered disulfide bonds. Protein Sci. 12, 997–1006.
19 Nguyen, V. T., Higuchi, H. and Kamio, Y. (2002) Controlling pore assembly of staphylococcal gamma-haemolysin by low temperature and by disulphide bond formation in double-cysteine LukF mutants. Mol. Microbiol. 45, 1485–1498.
20 Chattopadhyay, K. and Banerjee, K. K. (2003) Unfolding of *Vibrio cholerae* hemolysin induces oligomerization of the toxin monomer. J. Biol. Chem. 278, 38470–38475.
21 Kristan, K., Podlesek, Z., Hojnik, V., Gutierrez-Aguirre, I., Guncar, G., Turk, D., Gonzalez-Manas, J. M., Lakey, J. H., Macek, P. and Anderluh, G. (2004) Pore formation by equinatoxin, a eukaryotic pore-forming toxin, requires a flexible N-terminal region and a stable beta-sandwich. J. Biol. Chem. 279, 46509–46517.

22 Baba-Moussa, L., Werner, S., Colin, D. A., Mourey, L., Pédelacq, J. D., Samama, J. P., Sanni, A., Monteil, H. and Prévost, G. (1999) Discoupling the Ca^{2+}-activation from the pore-forming function of the bi-component Panton-Valentine leucocidin in human PMNs. FEBS Lett., 461, 280–286.

23 Werner, S., Colin, D. A., Coraiola, M., Menestrina, G., Monteil, H. and Prévost, G. (2002) Retrieving biological activity from LukF-PV mutants combined with different S-components implies compatibility between stem domains of these staphylococcal bi-component leucotoxins. Infect. Immun. 70, 1310–1318.

24 Ferreras, M., Hoeper, F., Dalla Serra, M., Colin, D.A., Prévost, G. and Menestrina, G. (1998) The interaction of *Staphylococcus aureus* bi-component gamma hemolysins and leucocidins with cells and model membranes. Biochim. Biophys. Acta 1414, 108–126.

25 Loo, T. W., Bartlett, M. C. and Clarke, D. M. (2004) Disulfide cross-linking analysis shows that transmembrane segments 5 and 8 of human P-glycoprotein are close together on the cytoplasmic side of the membrane. J. Biol. Chem. 279, 7692–7697.

26 Alvarez, C., Dalla Serra, M., Potrich, C., Bernhart, I., Tejuca, M., Martinez, D., Pazos, I. F., Lanio, M. E. and Menestrina, G. (2001) Effects of lipid composition on membrane permeabilization by Sticholysin I and II, two cytolysins of the sea anemone *Stichodactyla helianthus*, Biophys. J. 80, 2761–2774.

27 Dalla Serra, M. and Menestrina, G. (2000) Characterisation of molecular properties of pore-forming toxins with planar lipid bilayers. In: Holst, O. (ed.), Bacterial Toxins, Methods and Protocols, pp. 171–188, Humana Press, Totowa, NJ.

28 Gerstein, M., Lesk, A. M. and Chothia, C. (1994) Structural mechanisms for domain movements in proteins. Biochemistry 33, 6739–6749.

29 Gerstein, M. and Chothia, C. (1999): Signal transduction: proteins in motion. Science 285, 1682–1683.

30 Katz, B. A. and Kossiakoff, A. (1986) The crystallographically determined structures of atypical strained disulfides engineered into subtilisin. J. Biol. Chem. 261, 15480–15485.

31 Comai, M., Dalla Serra, M., Coraiola, M., Werner, S., Colin, D. A., Prévost, G. and Menestrina, G. (2002) Protein engineering modulates the transport properties and ion selectivity of the pores formed by staphylococcal gamma-hemolysins in lipid membranes. Mol. Microbiol. 44, 1251–1268.

32 Menestrina, G. (1986) Ionic channels formed by *Staphylococcus aureus* alpha-toxin: voltage dependent inhibition by di- and trivalent cations. J. Membr. Biol. 90, 177–190.

33 Galdiero, S. and Gouaux, E. (2004) High resolution crystallographic studies of alpha-hemolysin-phospholipid complexes define heptamer-lipid head group interactions: implication for understanding protein-lipid interactions. Protein Sci. 13, 1503–1511.

34 Iacovache, I., Paumard, P., Scheib, H., Lesieur, C., Sakai, N., Matile, S., Parker, M. W. and van der Goot, F. G. (2006) A rivet model for channel formation by aerolysin-like pore-forming toxins EMBO J. 25, 457–466.

35 Wimley, W. C., Hristova, K., Ladokhin, A. S., Silvestro, L., Axelsen, P. H. and White, S. H. (1998) Folding of beta-sheet membrane proteins: a hydrophobic hexapeptide model. J. Mol. Biol. 277, 1091–1110.

36 Bishop, C. R., Walkenhorst, W. F. and Wimley, W. C. (2001) Folding of beta-sheets in membranes: specificity and promiscuity in peptide model systems. J. Mol. Biol. 309, 975–988.

37 Tamm, L. K., Hong, H. and Liang, B. (2004) Folding and assembly of beta-barrel membrane proteins. Biochim. Biophys. Acta 1666, 250–263.

38 Hotze, E. M., Heuck, A. P., Czajkowsky, D. M., Shao, Z., Johnson, A. E. and Tweten, R. K. (2002) Monomer-monomer interactions drive the prepore to pore conversion of a beta-barrel-forming cholesterol-dependent cytolysin. J. Biol. Chem. 277, 11597–11605.

39 Vécsey-Semjén, B., Lesieur, S., Mollby, R. and van der Goot, F. G. (1997) Conformational changes due to membrane binding and channel formation by staphylococcal alpha-toxin. J. Biol. Chem. 272, 5709–5717.

40 Valeva, A., Weisser, A., Walker, B., Kehoe, M., Bayley, H., Bhakdi, S. and Palmer, M. (1996) Molecular architecture of a toxin pore: a 15-residue sequence lines the transmembrane channel of staphylococcal alpha-toxin. EMBO J. 15, 1857–1864.

41 Qa'dan, M., Christensen, K. A., Zhang, L., Roberts, T. M. and Collier, R. J. (2005) Membrane insertion by anthrax protective antigen in cultured cells. Mol. Cell. Biol. 25, 5492–5498.

42 Tilley, S. J. and Saibil, H. R. (2006) The mechanism of pore formation by bacterial toxins. Curr. Opin. Struct. Biol. 16, 230–236.

43 Benson, E. L., Huynh, P. D., Finkelstein, A. and Collier, R. J. (1998) Identification of residues lining the anthrax protective antigen channel. Biochemistry 37, 3941–3948.

44 Olson, R. and Gouaux, E. (2005) Crystal structure of the *Vibrio cholerae* cytolysin (VCC) pro-toxin and its assembly into a heptameric transmembrane pore. J. Mol. Biol. 350, 997–1016.

45 Loo, T. W., Bartlett, M. C. and Clarke, D. M. (2003) Substrate-induced conformational changes in the transmembrane segments of human P-glycoprotein. Direct evidence for the substrate-induced fit mechanism for drug binding. J. Biol. Chem. 278, 13603–13606.

46 Loo, T. W. and Clarke, D. M. (2000) The packing of the transmembrane segments of human multidrug resistance P-glycoprotein is revealed by disulfide cross-linking analysis, J. Biol. Chem. 275, 5253–5256.